Nonlinear Dynamics of Adaptive Gun Head Jet System of Fire-Fighting Monitor

XIAOMING YUAN[1,2,3], **XUAN ZHU**[1,3], **CHU WANG**[1,3], **AND LIJIE ZHANG**[1,3]

[1]Hebei Key Laboratory of Heavy Machinery Fluid Power Transmission and Control, Yanshan University, Qinhuangdao 066004, China
[2]State Key Laboratory of Fluid Power and Mechatronic Systems, Zhejiang University, Hangzhou 310027, China
[3]Key Laboratory of Advanced Forging and Stamping Technology and Science, Ministry of Education of China, Yanshan University, Qinhuangdao 066004, China

Corresponding authors: Chu Wang (wangchu@stumail.ysu.edu.cn) and Lijie Zhang (zhangljys@126.com)

ABSTRACT The working medium of the adaptive gun head jet system of fire-fighting monitor is generally water containing a little bit of air. During the operation, the pressure pulsation of the fluid will cause the fluctuation of the equivalent stiffness of the gas-liquid mixed fluid, so that the motion of the fluid in the jet system has obvious nonlinear characteristics. In this paper, the nonlinear dynamic model of the jet system is established. The analytical expressions of the nonlinear vibration response of the jet system are derived via the multi-scale method. The main resonance and combined resonance of the jet system are determined. The results show that the external excitation frequency is the dominant frequency of the main resonance response of the jet system, and the combined frequency between the natural frequency of each order and the equivalent stiffness fluctuation frequency of the fluid unit has a small effect on the main resonance, and the maximum amplitude is 0.2592mm; the dominant frequency of the combined resonance response of the jet system is the combined frequency between the natural frequency of each order and the equivalent stiffness fluctuation frequency of the fluid unit, the system amplitude in combined resonance is smaller than that in the main resonance, and the maximum amplitude is 0.002532mm; the main resonance and the combined resonance will adversely affect the dynamic characteristics of the jet system. This research can provide a theoretical basis for the dynamic optimization of the adaptive gun head jet system of the fire-fighting monitor.

INDEX TERMS Fire-fighting monitor, adaptive gun head, jet system, nonlinear vibration, dynamics.

I. INTRODUCTION

The nozzle opening of the adaptive gun head of the fire-fighting monitor can be adjusted according to the inlet flow and pressure of the jet system, so that the fire-fighting monitor can operate in optimal condition under various flows and extinguish large fires quickly and efficiently [1]. The working medium of the fire-fighting monitor is generally water containing a little bit of air. When the fire pump converts the mechanical energy of the prime mover into the kinetic energy of the fluid, it is likely that the air will be released because the pressure is lower than the air apart pressure. Meanwhile, a certain amount of air foam is often mixed at the entrance or exit of the fire pump to enhance the effect of

The associate editor coordinating the review of this manuscript and approving it for publication was Lei Wang.

fire extinguishing. Therefore, the jet fluid of the fire monitor is actually water containing a little bit of air, i.e. a gas-liquid mixed fluid. During the operation, the pulsation of both the flow and pressure of the fire pump inevitably causes the bulk modulus and stiffness of the jet fluid to constantly change. The stiffness of the gas-liquid mixed fluid determines the natural frequency of the fluid transmission system and directly affects the static and dynamic performance [2]. Since the fluid state parameters change periodically caused by the fluid compressibility and pressure pulsation, the jet system is a non-autonomous system and has obvious nonlinear characteristics.

The pressure pulsation of the jet system mainly comes from the pulsation of the fire pump itself. The fluid in the pump has two different types of pressure pulsations, namely turbulent pulsations that ignore the compressibility of the

fluid and pulse pulsations that ignore the viscosity of the fluid. It is generally considered that turbulent pulsations are random pulsations close to white noise, and pulse pulsations include harmonic signals, which are mainly composed of pulsations whose frequency is blade-passing frequency and harmonics, and pulsations whose frequency is rotation frequency and harmonics. The pressure pulsation of the fire pump is not only related to the rotation of the pump blades and shafts, but also affected by the cavitation and turbulence of the fluid. However, even the same fire pump still has pressure pulsations with different properties under different working conditions. Therefore, it is difficult to predict the pressure pulsations theoretically. With the popularization of computer technology, especially based on the development of computational fluid dynamics, modern intelligent fault diagnosis, digital signal processing and fast Fourier transform algorithm [3], [4], the multi-mode simulation and pulsation spectrum analysis of the internal flow field of the centrifugal pump have become a reality. Li *et al.* calculated the unsteady flow characteristics of the mixed-flow pump, analyzed the pressure pulsation characteristics of the mixed-flow pump under near stall conditions, and revealed the stall propagation mechanism [5]. Gao *et al.* analyzed the unsteady pressure pulsation and internal flow characteristics of the centrifugal pump, expounded the root cause of the periodic pressure pulsation, and pointed out that the interaction between the impeller and the volute tongue has a significant effect on the unsteady pressure pulsation of the centrifugal pump [6]. Zhang experimentally studied the effect of blade cutting on pump performance, especially the effect of pressure pulsation, and discussed the relationship between internal flow and pressure pulsation by numerical calculation [7]. Through experiments and numerical simulations, Appiah *et al.* verified that the instability of internal flow field during the rotation of the centrifugal pump impeller was the main factor causing the pressure pulsation, and pointed out that the rotor-stator interaction generated the highest pressure pulsation distribution at the volute tongue [8].

Aiming at the nonlinear dynamics of non-autonomous systems, scholars focus on applying nonlinear dynamic theory and methods to study the nonlinear vibration law, such as bifurcation and chaos, when random parameters change [9], [10]. The perturbation method, including the Krylov-Bogolubov-Mitropolsky (KBM) method, the harmonic balance method, and the multi-scale method, is often adopted in parametric vibration research, which can be directly used to solve the system's nonlinear differential equations [11], [12]. Moreover, the homotopy analysis method based on the continuously changing topological theory, is often used in analysis of strong nonlinear systems [13]. Liu *et al.* studied the nonlinear damped vibration of a fabric membrane under impact loading through the KBM perturbation method [14]. Keleshteri and Jelovica applied the harmonic balance method along with the direct iterative approach to the research of the free vibration response of functionally graded porous (FGP) cylindrical panels [15].

Wang *et al.* established the nonlinear free vibration model of a cantilever beam considering the effects of gravity, and analyzed super-harmonic resonances by the time-domain multi-scale method and harmonic balance method [16]. Sadri *et al.* applied multi-scale method to analyze the primary and secondary resonance conditions of a cantilever beam with intermediate lumped masses [17]. Armand *et al.* analyzed the effect of fretting wear on the nonlinear dynamic behaviors of assembly structures by the multi-scale method [18]. Hao researched the forced responses, the main resonances, and the superharmonic resonances of electromechanical integrated magnetic gear (EIMG) system via the multi-scale method, and found that when the wave frequency was close to the natural frequency or twice/half the natural frequency of the derived EIMG system, strong resonance occurred [19], [20]. Odibat proposed an optimal homotopy analysis approach, which accelerated the convergence of series solutions and was expected to be adopted in nonlinear problems in fractional calculus [21]. In order to deal with the common nonlinear problems of fluid transmission systems, scholars have analyzed the nonlinear dynamic characteristics through amplitude-frequency diagrams, time histories, Fourier spectra, phase portraits, and Poincare maps, and studied the instability mechanism [22], [23]. Some researchers employed several control strategies, such as adaptive robust control [24], [25], active disturbance rejection control [26], and multilayer neural-networks [27], to improve the control accuracy of the transmission system, thereby reducing the impact of vibration on the dynamic performance of the system. There are also scholars who proposed a novel pump and valve combined electro-hydraulic system [28] to improve the static and dynamic performance of the transmission system via principle innovation.

In summary, there is a periodic pressure pulsation during the operation of the fire pump, and the pressure pulsation directly affects the stability of the jet system. Research on the parameter vibration of the adaptive gun head jet system of fire-fighting monitor considering the pressure pulsation of the fire pump, however, has not been carried out. Based on the assumption that the fluid pressure pulsation is a harmonic function, a dynamic model of the adaptive gun head jet system of fire-fighting monitor is established, and the main resonance and combined resonance response under the parameter vibration of the jet system are determined by the multi-scale method, which can provide a theoretical basis for dynamic optimization design of the jet system.

II. DYNAMIC MODEL OF THE JET SYSTEM

The structure of the adaptive gun head is shown in Fig. 1. The inlet of the gun head is on the left side and the outlet is on the right. The adaptive mechanism consisting of the spray core, the end cap, the core rod, and the spring is the core component of the adaptive gun head. The end cap and the core rod are fixedly connected to the enclosure through the regulator. The spray core can slide in the axial direction. The left side of the spring acts on the spray core and the right
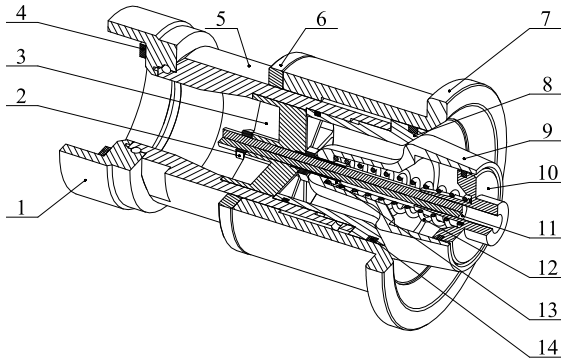
FIGURE 1. Structure of adaptive gun head. 1. Joint, 2. Nut, 3. Regulator, 4. Gasket, 5. Enclosure, 6. Ring, 7. Outer nozzle, 8. Inner nozzle, 9. Spray core, 10. End cap, 11. Core rod, 12. Spring, 13. Core sleeve, 14. Seal ring.
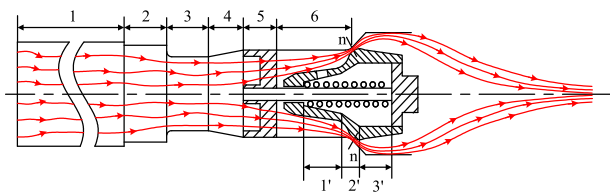

FIGURE 2. Internal structure of the adaptive gun head of the fire-fighting monitor.

TABLE 1. Internal structure size of the adaptive gun head of the fire-fighting monitor.

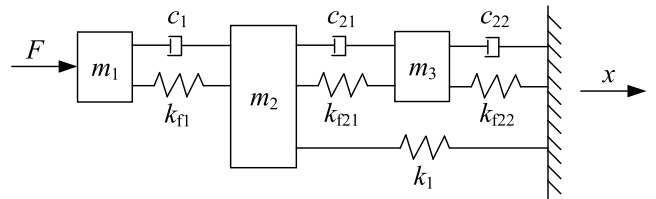| Fluid unit	Segmentation	Average area of flow cross section S_a/(mm^2)	Axial length of the fluid domain l/mm
Fluid unit 1	1	6221	1534.6
	2	6200	38
	3	3200	39
	4	3800	35.5
	5	4400	38
	6	3700	64
Fluid unit 2	1'	300	46.1
	2'	800	11
	3'	2800	40.5

FIGURE 3. Dynamic model of the adaptive gun head jet system of the fire-fighting monitor.

side acts on the end cap. At the initial moment, the spring is in a pre-compressed state. Meanwhile, the spray core is closely attached to the inner nozzle and the nozzle opening is zero. When the nozzle inlet flow increases, the force on the left side of the spray core increases. When the fluid force is greater than the spring force, the spray core moves to the right, and the nozzle opening increases. In contrast, when the inlet flow decreases, the spray core moves to the left, and the nozzle opening decreases. The adaptive mechanism enables the adaptive gun head to automatically adjust the nozzle opening according to the changes of inlet flow and pressure, so that it can achieve better jet performance under various operating conditions, and extinguish large fires quickly and efficiently.

The internal structure of the adaptive gun head of the fire-fighting monitor is shown in Fig. 2, and the pipe sections and their cross-sectional dimensions are shown in Table 1.

In Fig. 2, the red line with arrows is the flow line of the fluid. It can be known from the direction of the line that after flowing through the section n-n, where the nozzle opening locates, the fluid is reflected by the internal surface of the outer nozzle and converges at the front end of the gun head to form a jet. The regulator, installed at the fifth section of the gun head as shown in both Fig. 2 and Table 1, can turn the radial velocity of the fluid into the axial velocity, make the flow line more regular, and improve the stability of the jet. At the center of the spray core guidance surface, there are circular holes distributed evenly along the circle. During the operation of the fire-fighting monitor, the fluid enters the

interior of the spray core through circular holes and forms a certain hydrostatic pressure.

In order to facilitate theoretical modeling and analysis, the dynamic model of the adaptive gun head jet system of fire-fighting monitor makes the following assumptions:

1. Except the fluid unit and the spring, the parts such as the spray core and the enclosure are considered to be rigid bodies and their deformation is not considered.

2. The spray core and the fluid are only subjected to the axial force, and the force of the fluid on the spray core is simplified to the spring force along the axial direction.

3. The damping between the fluid unit and the solid element is equivalent to the axial linear damping, and the damping formed by the uniformly distributed small hole on the nozzle is equivalent to the axial linear damping.

4. Processing and installation errors of all parts are ignored.

The established dynamic model of the adaptive gun head jet system of the fire-fighting monitor is shown in Fig. 3.

In Fig. 3, F is the pulsating excitation force caused by the pressure fluctuation of the fire pump. m_1, m_2, and m_3 are the masses of the fluid unit 1, the spray core and the fluid unit 2 in the jet system, respectively. The fluid unit 1 is the fluid contained by the inlet flow cross section, the outer surface of the spray core, and the flow cross section n-n of the jet system, along with the internal surface of the fire-fighting monitor parts. The fluid unit 2 is the fluid contained by the inner surface of the spray core and the left end surface of the end cap. k_{f1} is the stiffness of fluid unit 1. k_{f21} is equal to k_{f22}, the total stiffness obtained by paralleling the two is the stiffness of fluid unit 2. k_1 is the stiffness of the mechanical spring inside the spray core. c_1 is the equivalent linear damping

between the pipe wall and the outer wall of the monitor and the fluid unit 1 in the jet system. c_2 is equal to c_3, and the total damping obtained by paralleling the two is equivalent to the structural damping of the orifice of the spray core.

III. DERIVATION AND SOLUTION OF VIBRATION EQUATION OF JET SYSTEM

A. TIME-VARYING EQUIVALENT STIFFNESS OF FLUID

In the dynamic model shown in Fig. 3, the stiffness of the fluid unit needs to be calculated equivalently. According to the bulk modulus theory of the gas-liquid mixed fluid, let Bf represents the bulk modulus of the gas-liquid mixed fluid, then we can get:

$$B_f = -\frac{V \Delta p}{\Delta V} \tag{1}$$

Assuming that the average area of the flow section of the fluid unit is S_a and the axial length of the fluid domain is l, then the volume of the fluid domain is:

$$V = S_a l \tag{2}$$

The definition of stiffness is:

$$k_f = -\frac{\Delta F}{\Delta l} \tag{3}$$

Combining (1), (2), and (3), the fluid equivalent stiffness can be expressed with the fluid bulk modulus as:

$$k_f = \frac{B_f S_a}{l} \tag{4}$$

During the operation, the pulsation of the flow and pressure of the fire pump is inevitable, so the fluid density and equivalent stiffness constantly change. Under actual working conditions, the fluid pressure consists of two parts: average pressure and pulsating pressure. Assuming that the pulsating pressure varies by cosine, according to Euler's theorem, the time-varying pressure pulsation can be expressed as:

$$p = \bar{p} + \Delta p \left(e^{j\omega_o t} + e^{-j\omega_o t} \right) \tag{5}$$

where $\bar{p}$ is steady pressure, Δp is the pressure pulsation amplitude (Pa), and ω_o is the pressure pulsation angular frequency (rad/s).

Under a certain initial gas content, the fluctuation of the equivalent fluid stiffness is consistent with the fluid pressure and can be expressed as:

$$k_{fi} = \bar{k}_{fi} + \Delta k_{fi} \cos \omega_f t = \bar{k}_{fi} \left(1 + \varepsilon e^{j\omega_f t} + \varepsilon e^{-j\omega_f t} \right) \tag{6}$$

where $i = 1, 2$, $\bar{k}_{fi}$ is the steady equivalent stiffness of the fluid unit (N/m), Δk_{fi} is the equivalent stiffness fluctuation of the fluid unit (N/m), ε is a small parameter and $\varepsilon = \Delta k_{fi}/2\bar{k}_{fi}$, ω_f is the time-varying equivalent stiffness angular frequency of the fluid unit (rad/s).

B. PARAMETRIC VIBRATION EQUATION OF JET SYSTEM

Based on the lumped parameter method, k_{f2} represents paralleled k_{f21} and k_{f22}, and the parametric vibration equation obtained from the dynamic model of the jet system shown in Fig. 3 is:

$$M\ddot{x} + C\dot{x} + Kx = \Delta F - \Delta Kx \tag{7}$$

where the mass matrix is:

$$M = \begin{bmatrix} m'_1 & & \\ & m'_2 & \\ & & m'_3 \end{bmatrix} \tag{8}$$

The damping matrix is:

$$C = \begin{bmatrix} c_1 & -c_1 & 0 \\ -c_1 & c_1 + c_2 & -c_2 \\ 0 & -c_2 & c_2 + c_3 \end{bmatrix} \tag{9}$$

The stiffness matrix is:

$$K = \begin{bmatrix} k_{f1} & -k_{f1} & 0 \\ -k_{f1} & k_{f1} + \dfrac{k_{f2}}{2} + k_1 & -\dfrac{k_{f2}}{2} \\ 0 & -\dfrac{k_{f2}}{2} & k_{f2} \end{bmatrix} \tag{10}$$

Under stable operation, the equivalent stiffness of the two fluid units and the external force on the jet system vary by cosine. According to Euler's formula, the time-varying external excitation of a jet system can be expressed as:

$$\Delta F = \left[F \frac{\left(e^{j\omega_o t} + e^{-j\omega_o t} \right)}{2} \quad 0 \quad 0 \right]^T \tag{11}$$

The stiffness fluctuation matrix is:

$$\Delta K = \varepsilon \left(e^{j\omega_f t} + e^{-j\omega_f t} \right) \begin{bmatrix} \bar{k}_{f1} & -\bar{k}_{f1} & 0 \\ -\bar{k}_{f1} & \bar{k}_{f1} + \dfrac{\bar{k}_{f2}}{2} & -\dfrac{\bar{k}_{f2}}{2} \\ 0 & -\dfrac{\bar{k}_{f2}}{2} & \bar{k}_{f2} \end{bmatrix} \tag{12}$$

The regular mode ψ and the spectral matrix Λ of the system are known, after the regularization of (7), we can obtain:

$$\ddot{\eta} + C_N \dot{\eta} + \Lambda \eta = \Delta Q - \Delta K_N \eta \tag{13}$$

where η is the regular displacement vector, C_N is the regular damping matrix, ΔQ is the regular external excitation vector and ΔK_N is the regular equivalent stiffness fluctuation matrix of the fluid unit.

Among them, C_N is:

$$C_N = \begin{bmatrix} c_{N11} & c_{N12} & c_{N13} \\ c_{N21} & c_{N22} & c_{N23} \\ c_{N31} & c_{N32} & c_{N33} \end{bmatrix} \tag{14}$$

ΔQ can be expressed as:

$$\Delta Q = F \frac{\left(e^{j\omega_f t} + e^{-j\omega_f t} \right)}{2} \begin{bmatrix} \psi_{1,1} & \psi_{1,2} & \psi_{1,3} \end{bmatrix}^T \tag{15}$$

And $\Delta \boldsymbol{K}_N$ is:

$$\Delta \boldsymbol{K}_N = \varepsilon \left(e^{j\omega_f t} + e^{-j\omega_f t} \right) \begin{bmatrix} \Delta k_{N11} & \Delta k_{N12} & \Delta k_{N13} \\ \Delta k_{N21} & \Delta k_{N22} & \Delta k_{N23} \\ \Delta k_{N31} & \Delta k_{N32} & \Delta k_{N33} \end{bmatrix} \tag{16}$$

C. APPROXIMATE ANALYTICAL SOLUTION OF THE MAIN RESONANCE OF JET SYSTEM

Based on the multi-scale method, the quadratic approximate solution and small parameter are introduced:

$$\begin{cases} \eta_i = \eta_{i0}(T_0, T_1) + \varepsilon \eta_{i1}(T_0, T_1) + \cdots \\ c_{Nij} = \varepsilon c'_{Nij} \\ F = \varepsilon F' \end{cases} \tag{17}$$

where $T_0 = t$, $T_1 = \varepsilon t$, and values of i and j are 1, 2, and 3, respectively.

Substituting the above equations into (13), we can get the zero power equation of ε:

$$\begin{cases} \dfrac{\partial^2 \eta_{10}}{\partial T_0^2} + \omega_{n1}^2 \eta_{10} = 0 \\ \dfrac{\partial^2 \eta_{20}}{\partial T_0^2} + \omega_{n2}^2 \eta_{20} = 0 \\ \dfrac{\partial^2 \eta_{30}}{\partial T_0^2} + \omega_{n3}^2 \eta_{30} = 0 \end{cases} \tag{18}$$

And the first power equation of ε is:

$$\begin{cases} \dfrac{\partial^2 \eta_{11}}{\partial T_0^2} + \omega_{n1}^2 \eta_{11} \\ = -2\dfrac{\partial^2 \eta_{10}}{\partial T_0 \partial T_1} + \dfrac{F' e^{j\omega_o t}}{2} \psi_{1,1} \\ \quad - \left(c'_{N11} \dfrac{\partial \eta_{10}}{\partial T_0} + c'_{N12} \dfrac{\partial \eta_{20}}{\partial T_0} + c'_{N13} \dfrac{\partial \eta_{30}}{\partial T_0} \right) \\ \quad - e^{j\omega_f t}(\Delta k_{N11}\eta_{10} + \Delta k_{N12}\eta_{20} + \Delta k_{N13}\eta_{30}) + cc \\[6pt] \dfrac{\partial^2 \eta_{21}}{\partial T_0^2} + \omega_{n2}^2 \eta_{21} \\ = -2\dfrac{\partial^2 \eta_{20}}{\partial T_0 \partial T_1} + \dfrac{F' e^{j\omega_o t}}{2} \psi_{1,2} \\ \quad - \left(c'_{N21} \dfrac{\partial \eta_{10}}{\partial T_0} + c'_{N22} \dfrac{\partial \eta_{20}}{\partial T_0} + c'_{N23} \dfrac{\partial \eta_{30}}{\partial T_0} \right) \\ \quad - e^{j\omega_f t}(\Delta k_{N21}\eta_{10} + \Delta k_{N22}\eta_{20} + \Delta k_{N23}\eta_{30}) + cc \\[6pt] \dfrac{\partial^2 \eta_{31}}{\partial T_0^2} + \omega_{n3}^2 \eta_{31} \\ = -2\dfrac{\partial^2 \eta_{30}}{\partial T_0 \partial T_1} + \dfrac{F' e^{j\omega_o t}}{2} \psi_{1,3} \\ \quad - \left(c'_{N31} \dfrac{\partial \eta_{10}}{\partial T_0} + c'_{N32} \dfrac{\partial \eta_{20}}{\partial T_0} + c'_{N33} \dfrac{\partial \eta_{30}}{\partial T_0} \right) \\ \quad - e^{j\omega_f t}(\Delta k_{N31}\eta_{10} + \Delta k_{N32}\eta_{20} + \Delta k_{N33}\eta_{30}) + cc \end{cases} \tag{19}$$

where, cc is the complex conjugate.

Let the solution of (18) be:

$$\eta_{i0} = A_i e^{j\omega_{ni} T_0} + cc \tag{20}$$

where, $i = 1$, 2, and 3.

The following equation can be obtained by substituting (20) into (19):

$$\begin{cases} \dfrac{\partial^2 \eta_{11}}{\partial T_0^2} + \omega_{n1}^2 \eta_{11} \\ = -j\omega_{n1} \left(2\dfrac{dA_1}{dT_1} + c'_{N11}A_1 \right) e^{j\omega_{n1} T_0} + \dfrac{F' e^{j\omega_o t}}{2} \psi_{1,1} \\ \quad - (c'_{N12} j\omega_{n2} A_2 e^{j\omega_{n2} T_0} + c'_{N13} j\omega_{n3} A_3 e^{j\omega_{n3} T_0}) \\ \quad - \left(\begin{matrix} \Delta k_{N11} A_1 e^{j(\omega_{n1}+\omega_f)T_0} + \Delta k_{N12} A_2 e^{j(\omega_{n2}+\omega_f)T_0} + \\ \Delta k_{N13} A_3 e^{j(\omega_{n3}+\omega_f)T_0} \end{matrix} \right) + cc \\[10pt] \dfrac{\partial^2 \eta_{21}}{\partial T_0^2} + \omega_{n2}^2 \eta_{21} \\ = -j\omega_{n2} \left(2\dfrac{dA_2}{dT_1} + c'_{N22}A_2 \right) e^{j\omega_{n2} T_0} + \dfrac{F' e^{j\omega_o t}}{2} \psi_{1,2} \\ \quad - (c'_{N21} j\omega_{n1} A_1 e^{j\omega_{n1} T_0} + c'_{N23} j\omega_{n3} A_3 e^{j\omega_{n3} T_0}) \\ \quad - \left(\begin{matrix} \Delta k_{N21} A_1 e^{j(\omega_{n1}+\omega_f)T_0} + \Delta k_{N22} A_2 e^{j(\omega_{n2}+\omega_f)T_0} + \\ \Delta k_{N23} A_3 e^{j(\omega_{n3}+\omega_f)T_0} \end{matrix} \right) + cc \\[10pt] \dfrac{\partial^2 \eta_{31}}{\partial T_0^2} + \omega_{n3}^2 \eta_{31} \\ = -j\omega_{n3} \left(2\dfrac{dA_3}{dT_1} + c'_{N33}A_3 \right) e^{j\omega_{n3} T_0} + \dfrac{F' e^{j\omega_o t}}{2} \psi_{1,3} \\ \quad - (c'_{N31} j\omega_{n1} A_1 e^{j\omega_{n1} T_0} + c'_{N32} j\omega_{n2} A_2 e^{j\omega_{n2} T_0}) \\ \quad - \left(\begin{matrix} \Delta k_{N31} A_1 e^{j(\omega_{n1}+\omega_f)T_0} + \Delta k_{N32} A_2 e^{j(\omega_{n2}+\omega_f)T_0} + \\ \Delta k_{N33} A_3 e^{j(\omega_{n3}+\omega_f)T_0} \end{matrix} \right) + cc \end{cases} \tag{21}$$

When the external excitation frequency of is close to the first natural frequency of the jet system, the main resonance of the jet system will occur. After introducing the tuning parameter σ, ω_o can be expressed as:

$$\omega_o = \omega_{n1} + \varepsilon \sigma \tag{22}$$

After substituting (22) into (21), we need to eliminate the secular term, so:

$$\begin{cases} -j\omega_{n1} \left(2\dfrac{dA_1}{dT_1} + c'_{N11}A_1 \right) + F' \psi_{1,1} \dfrac{e^{j\sigma T_1}}{2} = 0 \\ -j\omega_{n2} \left(2\dfrac{dA_2}{dT_1} + c'_{N22}A_2 \right) = 0 \\ -j\omega_{n3} \left(2\dfrac{dA_3}{dT_1} + c'_{N33}A_3 \right) = 0 \end{cases} \tag{23}$$

Equation (23) can be solved by method of variation of constant, and the solution is:

$$\begin{cases} A_1 = C_1 e^{-\frac{c'_{N11}}{2} T_1} + \dfrac{F' \psi_{1,1}}{j2\omega_{n1}(2j\sigma + c'_{N11})} e^{j\sigma T_1} \\ A_2 = C_2 e^{-\frac{c'_{N22}}{2} T_1} \\ A_3 = C_3 e^{-\frac{c'_{N33}}{2} T_1} \end{cases} \tag{24}$$

where C_i ($i = 1, 2, 3$) is a constant determined by the initial conditions of the jet system.

The first formula in (23) can be simplified by combining trigonometric function, complex number, and Euler's formula:

$$A_1 = C_1 e^{-\frac{c'_{N11}}{2}T_1} - \frac{F'\psi_{1,1}}{2\omega_{n1}\sqrt{\left(c'_{N11}\right)^2 + 4\sigma^2}}e^{j(\theta+\sigma T_1)} \quad (25)$$

where $\theta = \arctan\left(\frac{c'_{N11}}{2\sigma}\right)$.

The term $C_i e^{-\frac{c'_{Nii}}{2}T_1}$ in (24) will gradually approach zero over time, so the steady zero-order approximate analytical solution of the jet system can be obtained by substituting (24) into (20):

$$\begin{cases} \eta_{10} = -\dfrac{F'\psi_{1,1}}{\omega_{n1}\sqrt{\left(c'_{N11}\right)^2 + 4\sigma^2}}\cos\left(\theta + (\omega_{n1} + \varepsilon\sigma)t\right) \\ \eta_{20} = 0 \\ \eta_{30} = 0 \end{cases} \quad (26)$$

The steady first-order approximate analytical solution of the jet system can be obtained by substituting (24) and (25) into (21):

$$\begin{cases} \eta_{11} = -2\Delta k_{N11}A_1\left[\begin{array}{l} \dfrac{\cos(\omega_{n1}-\omega_f)t}{\omega_f(2\omega_{n1}-\omega_f)} \\ -\dfrac{\cos(\omega_{n1}+\omega_f)t}{\omega_f(2\omega_{n1}+\omega_f)} \end{array}\right] \\ \eta_{21} = \dfrac{F'_o\psi_{1,2}\cos(\omega_o t)}{\omega_{n2}^2 - \omega_o^2} \\ \qquad -2\left[\begin{array}{l} \Delta k_{N21}A_1\left(\begin{array}{l}\dfrac{\cos(\omega_{n1}+\omega_f)t}{\omega_{n2}^2 - (\omega_{n1}+\omega_f)^2} \\ +\dfrac{\cos(\omega_{n1}-\omega_f)t}{\omega_{n2}^2 - (\omega_{n1}-\omega_f)^2}\end{array}\right) \\ -\dfrac{c'_{N21}\omega_{n1}A_1\sin\omega_{n1}t}{\omega_{n2}^2 - \omega_{n1}^2} \end{array}\right] \\ \eta_{31} = \dfrac{F'_o\psi_{1,3}\cos(\omega_o t)}{\omega_{n3}^2 - \omega_o^2} \\ \qquad -2\left[\begin{array}{l} \Delta k_{N31}A_1\left(\begin{array}{l}\dfrac{\cos(\omega_{n1}+\omega_f)t}{\omega_{n3}^2 - (\omega_{n1}+\omega_f)^2} \\ +\dfrac{\cos(\omega_{n1}-\omega_f)t}{\omega_{n3}^2 - (\omega_{n1}-\omega_f)^2}\end{array}\right) \\ -\dfrac{c'_{N31}\omega_{n1}A_1\sin\omega_{n1}t}{\omega_{n3}^2 - \omega_{n1}^2} \end{array}\right] \end{cases} \quad (27)$$

Then the steady response of the main resonance of the jet system in rectangular coordinates is:

$$x = \psi\left(\eta_0 + \varepsilon\eta_1\right) \quad (28)$$

When the external excitation frequency approaches the second and third natural frequencies of the jet system respectively, the main resonance response can be obtained referring to the above solution process.

From the above results, it can be known that the main resonance response of the jet system includes multiple frequency components, including the first natural frequency, the second natural frequency, the third natural frequency,

the fluid equivalent stiffness fluctuation frequency, and the combination frequency of the natural frequency and the stiffness fluctuation frequency.

D. APPROXIMATE ANALYTICAL SOLUTION OF THE COMBINED RESONANCE OF JET SYSTEM

Similar to the derivation of the main resonance, the multi-scale method is also used to derive the combined resonance response of the jet system. The quadratic approximate solution and small parameter are introduced, then:

$$\begin{cases} \eta_i = \eta_{i0}(T_0, T_1) + \varepsilon\eta_{i1}(T_0, T_1) + \cdots \\ c_{Nij} = \varepsilon c'_{Nij} \end{cases} \quad (29)$$

where, $T_n = \varepsilon^n t$ and values of i and j are 1, 2, and 3, respectively.

Substituting (29) into (13), we can get the zero power equation of ε:

$$\begin{cases} \dfrac{\partial^2\eta_{10}}{\partial T_0^2} + \omega_{n1}^2\eta_{10} = \dfrac{F\psi_{1,1}}{2}e^{j\omega_o t} + cc \\ \dfrac{\partial^2\eta_{20}}{\partial T_0^2} + \omega_{n2}^2\eta_{20} = \dfrac{F\psi_{1,2}}{2}e^{j\omega_o t} + cc \\ \dfrac{\partial^2\eta_{30}}{\partial T_0^2} + \omega_{n3}^2\eta_{30} = \dfrac{F\psi_{1,3}}{2}e^{j\omega_o t} + cc \end{cases} \quad (30)$$

where cc is the complex conjugate.

And the first power equation of ε is:

$$\begin{cases} \dfrac{\partial^2\eta_{11}}{\partial T_0^2} + \omega_{n1}^2\eta_{11} \\ = -2\dfrac{\partial^2\eta_{10}}{\partial T_0\partial T_1} \\ \quad -e^{j\omega_f t}\left(\Delta k_{N11}\eta_{10} + \Delta k_{N12}\eta_{20} + \Delta k_{N13}\eta_{30}\right) \\ \quad -\left(c'_{N11}\dfrac{\partial\eta_{10}}{\partial T_0} + c'_{N12}\dfrac{\partial\eta_{20}}{\partial T_0} + c'_{N13}\dfrac{\partial\eta_{30}}{\partial T_0}\right) + cc \\ \dfrac{\partial^2\eta_{21}}{\partial T_0^2} + \omega_{n2}^2\eta_{21} \\ = -2\dfrac{\partial^2\eta_{20}}{\partial T_0\partial T_1} \\ \quad -e^{j\omega_f t}\left(\Delta k_{N21}\eta_{10} + \Delta k_{N22}\eta_{20} + \Delta k_{N23}\eta_{30}\right) \\ \quad -\left(c'_{N21}\dfrac{\partial\eta_{10}}{\partial T_0} + c'_{N22}\dfrac{\partial\eta_{20}}{\partial T_0} + c'_{N23}\dfrac{\partial\eta_{30}}{\partial T_0}\right) + cc \\ \dfrac{\partial^2\eta_{31}}{\partial T_0^2} + \omega_{n3}^2\eta_{31} \\ = -2\dfrac{\partial^2\eta_{30}}{\partial T_0\partial T_1} \\ \quad -e^{j\omega_f t}\left(\Delta k_{N31}\eta_{10} + \Delta k_{N32}\eta_{20} + \Delta k_{N33}\eta_{30}\right) \\ \quad -\left(c'_{N31}\dfrac{\partial\eta_{10}}{\partial T_0} + c'_{N32}\dfrac{\partial\eta_{20}}{\partial T_0} + c'_{N33}\dfrac{\partial\eta_{30}}{\partial T_0}\right) + cc \end{cases} \quad (31)$$

Let the solution of (30) be:

$$\eta_{i0} = B_i e^{j\omega_{ni}T_0} + D_i e^{j\omega_o T_0} + cc \quad (32)$$

where, $D_i = \dfrac{F\psi_{1,i}}{2(\omega_{ni}^2 - \omega_o^2)}$ and $i = 1, 2,$ and 3.

The following equation can be obtained by substituting (32) into (31):

$$
\begin{cases}
\begin{aligned}
&\frac{\partial^2 \eta_{11}}{\partial T_0^2} + \omega_{n1}^2 \eta_{11} \\
&= -2j\omega_{n1}\frac{dB_1}{dT_1}e^{j\omega_{n1}T_0} \\
&\quad - \begin{bmatrix} c'_{N11}\left(j\omega_{n1}B_1 e^{j\omega_{n1}T_0} + j\omega_o D_1 e^{j\omega_o T_0}\right) + \\ c'_{N12}\left(j\omega_{n2}B_2 e^{j\omega_{n2}T_0} + j\omega_o D_2 e^{j\omega_o T_0}\right) + \\ c'_{N13}\left(j\omega_{n3}B_3 e^{j\omega_{n3}T_0} + j\omega_o D_3 e^{j\omega_o T_0}\right) \end{bmatrix} \\
&\quad - \begin{bmatrix} \Delta k_{N11}\left(B_1 e^{j(\omega_{n1}+\omega_f)T_0} + D_1 e^{j(\omega_o+\omega_f)T_0}\right) \\ +\Delta k_{N12}\left(B_2 e^{j(\omega_{n2}+\omega_f)T_0} + D_2 e^{j(\omega_o+\omega_f)T_0}\right) \\ +\Delta k_{N13}\left(B_3 e^{j(\omega_{n3}+\omega_f)T_0} + D_3 e^{j(\omega_o+\omega_f)T_0}\right) \end{bmatrix} + cc \\[6pt]
&\frac{\partial^2 \eta_{21}}{\partial T_0^2} + \omega_{n2}^2 \eta_{21} \\
&= -2j\omega_{n2}\frac{dB_2}{dT_1}e^{j\omega_{n2}T_0} \\
&\quad - \begin{bmatrix} c'_{N21}\left(j\omega_{n1}B_1 e^{j\omega_{n1}T_0} + j\omega_o D_1 e^{j\omega_o T_0}\right) + \\ c'_{N22}\left(j\omega_{n2}B_2 e^{j\omega_{n2}T_0} + j\omega_o D_2 e^{j\omega_o T_0}\right) + \\ c'_{N23}\left(j\omega_{n3}B_3 e^{j\omega_{n3}T_0} + j\omega_o D_3 e^{j\omega_o T_0}\right) \end{bmatrix} \\
&\quad - \begin{bmatrix} \Delta k_{N21}\left(B_1 e^{j(\omega_{n1}+\omega_f)T_0} + D_1 e^{j(\omega_o+\omega_f)T_0}\right) \\ +\Delta k_{N22}\left(B_2 e^{j(\omega_{n2}+\omega_f)T_0} + D_2 e^{j(\omega_o+\omega_f)T_0}\right) \\ +\Delta k_{N23}\left(B_3 e^{j(\omega_{n3}+\omega_f)T_0} + D_3 e^{j(\omega_o+\omega_f)T_0}\right) \end{bmatrix} + cc \\[6pt]
&\frac{\partial^2 \eta_{31}}{\partial T_0^2} + \omega_{n3}^2 \eta_{31} \\
&= -2j\omega_{n3}\frac{dB_3}{dT_1}e^{j\omega_{n3}T_0} \\
&\quad - \begin{bmatrix} c'_{N31}\left(j\omega_{n1}B_1 e^{j\omega_{n1}T_0} + j\omega_o D_1 e^{j\omega_o T_0}\right) + \\ c'_{N32}\left(j\omega_{n2}B_2 e^{j\omega_{n2}T_0} + j\omega_o D_2 e^{j\omega_o T_0}\right) + \\ c'_{N33}\left(j\omega_{n3}B_3 e^{j\omega_{n3}T_0} + j\omega_o D_3 e^{j\omega_o T_0}\right) \end{bmatrix} \\
&\quad - \begin{bmatrix} \Delta k_{N31}\left(B_1 e^{j(\omega_{n1}+\omega_f)T_0} + D_1 e^{j(\omega_o+\omega_f)T_0}\right) \\ +\Delta k_{N32}\left(B_2 e^{j(\omega_{n2}+\omega_f)T_0} + D_2 e^{j(\omega_o+\omega_f)T_0}\right) \\ +\Delta k_{N33}\left(B_3 e^{j(\omega_{n3}+\omega_f)T_0} + D_3 e^{j(\omega_o+\omega_f)T_0}\right) \end{bmatrix} + cc
\end{aligned}
\end{cases}
\tag{33}
$$

According to (33), except that when the external excitation frequency is close to the natural frequencies of the jet system, the main resonance of the jet system will occur. When the external excitation frequency is close to the combined frequency between the natural frequency of each order and the equivalent stiffness fluctuation frequency of the fluid unit, the combined resonance of the jet system will also occur. The emergence of the main resonance and combined resonance makes the vibration of the jet system more complex and diverse.

When the external excitation frequency of is close to the first natural frequency of the jet system ω_{n1} and the equivalent stiffness fluctuation frequency of the fluid ω_f, after introducing the tuning parameter σ, ω_o can be expressed as:

$$
\omega_o = \omega_{n1} + \omega_f + \varepsilon\sigma \tag{34}
$$

TABLE 2. Parameters of adaptive gun head jet system of the fire-fighting monitor.

Parameter	Symbol	Unit	Value
Mass of fluid unit 1	m_1	kg	10.4
Mass of spray core	m_2	kg	0.32
Mass of fluid unit 2	m_3	kg	0.14
Steady value of dynamic bulk modulus of gas-liquid mixed fluid	B_f	Mpa	161.92
Fluctuating value of dynamic bulk modulus of gas-liquid mixed fluid	ΔB_f	Mpa	0.34
Equivalent stiffness steady value of fluid unit 1	$\bar{k}_{f1}$	kN/m	541.15
Equivalent stiffness fluctuating value of fluid unit 1	Δk_{f1}	kN/m	1.14
Equivalent stiffness steady value of fluid unit 2	$\bar{k}_{f2}$	kN/m	852.22
Equivalent stiffness fluctuating value of fluid unit 2	Δk_{f2}	kN/m	1.79
Equivalent stiffness fluctuating frequency of fluid units	ω_f	rad·s⁻¹	294.01
Stiffness of mechanical spring	k_5	kN/m	18
External excitation amplitude	F	N	4.26
Fluid damping	c_1	N·(m/s)⁻¹	0.01
Structural damping	c_2	N·(m/s)⁻¹	0.05

After substituting (34) into (33), we need to eliminate the secular term, so:

$$
\begin{cases}
\begin{aligned}
&j\omega_{n1}\left(2\frac{dB_1}{dT_1} + c'_{N11}B_1\right) \\
&\quad + (\Delta k_{N11}D_1 + \Delta k_{N12}D_2 + \Delta k_{N13}D_3)\,e^{j\sigma T_1} = 0 \\
&j\omega_{n2}\left(2\frac{dB_2}{dT_1} + c'_{N22}B_2\right) = 0 \\
&j\omega_{n3}\left(2\frac{dB_3}{dT_1} + c'_{N33}B_3\right) = 0
\end{aligned}
\end{cases}
\tag{35}
$$

Equation (35) can be solved by method of variation of constant, and the solution is:

$$
\begin{cases}
B_1 = E_1 e^{-\frac{c'_{N11}}{2}T_1} + \dfrac{(\Delta k_{N11}D_1 + \Delta k_{N12}D_2 + \Delta k_{N13}D_3)}{\omega_{n1}\sqrt{4\sigma^2 + (c'_{N11})^2}} e^{j(\theta+\sigma T_1)} \\
B_2 = E_2 e^{-\frac{c'_{N22}}{2}T_1} \\
B_3 = E_3 e^{-\frac{c'_{N33}}{2}T_1}
\end{cases}
\tag{36}
$$

where E_i $(i = 1, 2, 3)$ is a constant determined by the initial conditions of the jet system, and $\theta = \arctan\left(\frac{c'_{N11}}{2\sigma}\right)$.

The steady zero-order approximate analytical solution of the jet system can be obtained by substituting (36) into (32):

$$
\begin{cases}
\begin{aligned}
\eta_{10} &= 2\dfrac{(\Delta k_{N11}D_1 + \Delta k_{N12}D_2 + \Delta k_{N13}D_3)}{\omega_{n1}\sqrt{4\sigma^2 + (c'_{N11})^2}} \\
&\quad \cos\left(\theta + (\omega_{n1} + \varepsilon\sigma)\,t\right) + 2D_1\cos\omega_o t \\
\eta_{20} &= 2D_2\cos\omega_o t \\
\eta_{30} &= 2D_3\cos\omega_o t
\end{aligned}
\end{cases}
\tag{37}
$$

The steady first-order approximate analytical solution of the jet system can be obtained by substituting (36) into (33):

$$
\begin{cases}
\eta_{11} \\
= -2 \left[\Delta k_{N11} B_1 \left(\dfrac{\cos(\omega_{n1}-\omega_f)\,t}{\omega_f(2\omega_{n1}-\omega_f)} - \dfrac{\cos(\omega_{n1}+\omega_f)\,t}{\omega_f(2\omega_{n1}+\omega_f)} \right) + \dfrac{(\Delta k_{N11}D_1 + \Delta k_{N12}D_2 + \Delta k_{N13}D_3)\cos(\omega_o+\omega_f)\,t}{(\omega_{n1}^2 - (\omega_o+\omega_f)^2)} - \dfrac{\omega_o(c'_{N11}D_1 + c'_{N12}D_2 + c'_{N13}D_3)\sin\omega_o t}{(\omega_{n1}^2 - \omega_o^2)} \right] \\[2mm]
\eta_{21} \\
= -2 \left[\Delta k_{N21} B_1 \left(\dfrac{\cos(\omega_{n1}+\omega_f)\,t}{\omega_{n2}^2 - (\omega_{n1}+\omega_f)^2} + \dfrac{\cos(\omega_{n1}-\omega_f)\,t}{\omega_{n2}^2 - (\omega_{n1}-\omega_f)^2} \right) + (\Delta k_{N21}D_1 + \Delta k_{N22}D_2 + \Delta k_{N23}D_3)\left(\dfrac{\cos(\omega_o+\omega_f)\,t}{\omega_{n2}^2 - (\omega_o+\omega_f)^2} + \dfrac{\cos(\omega_o-\omega_f)\,t}{\omega_{n2}^2 - (\omega_o-\omega_f)^2} \right) - \dfrac{\omega_o(c'_{N21}D_1 + c'_{N22}D_2 + c'_{N23}D_3)\sin\omega_o t}{\omega_{n2}^2 - \omega_o^2} - \dfrac{\omega_{n1}c'_{N21}B_1 \sin\omega_{n1}t}{\omega_{n2}^2 - \omega_{n1}^2} \right] \\[2mm]
\eta_{31} \\
= -2 \left[\Delta k_{N31} B_1 \left(\dfrac{\cos(\omega_{n1}+\omega_f)\,t}{\omega_{n3}^2 - (\omega_{n1}+\omega_f)^2} + \dfrac{\cos(\omega_{n1}-\omega_f)\,t}{\omega_{n3}^2 - (\omega_{n1}-\omega_f)^2} \right) + (\Delta k_{N31}D_1 + \Delta k_{N32}D_2 + \Delta k_{N33}D_3)\left(\dfrac{\cos(\omega_o+\omega_f)\,t}{\omega_{n3}^2 - (\omega_o+\omega_f)^2} + \dfrac{\cos(\omega_o-\omega_f)\,t}{\omega_{n3}^2 - (\omega_o-\omega_f)^2} \right) - \dfrac{\omega_o(c'_{N31}D_1 + c'_{N32}D_2 + c'_{N33}D_3)\sin\omega_o t}{\omega_{n3}^2 - \omega_o^2} - \dfrac{\omega_{n1}c'_{N31}B_1 \sin\omega_{n1}t}{\omega_{n3}^2 - \omega_{n1}^2} \right]
\end{cases}
\tag{38}
$$

Then the steady response of the combined resonance of the jet system in rectangular coordinates is:

$$
\boldsymbol{x} = \boldsymbol{\psi}\left(\boldsymbol{\eta}_0 + \varepsilon \boldsymbol{\eta}_1 \right)
\tag{39}
$$

When the external excitation frequency approaches the combined frequency between the natural frequencies of the second and third order and the equivalent stiffness fluctuation frequency of the fluid unit respectively, the combined resonance response can be obtained referring to the above solution process.

IV. ANALYSIS OF PARAMETRIC VIBRATION RESPONSE OF JET SYSTEM

The time-domain response of the jet system can be determined based on the time-domain theory, and the amplitude-frequency characteristics of the jet system can be determined by Fourier transform. The parameters of adaptive gun head jet system of the fire-fighting monitor are shown in Table 2.

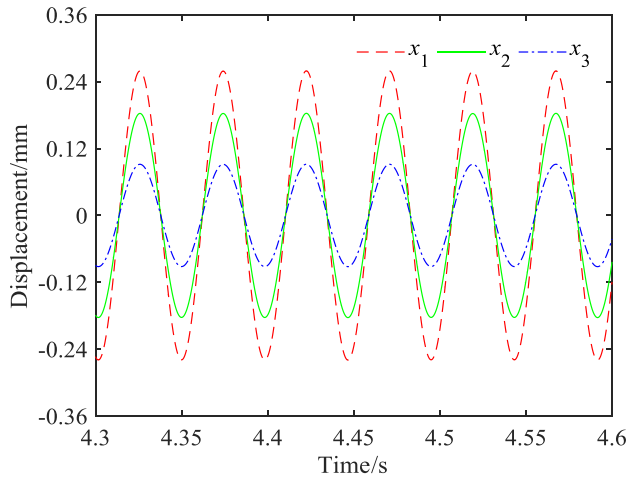### A. ANALYSIS OF THE MAIN RESONANCE RESPONSE OF JET SYSTEM

When the external excitation frequencies are close to the stable values of the natural angular frequency of each order of the jet system, the time domain response and the frequency domain response of the jet system are shown in Fig. 4 and Fig. 5, respectively.

It can be seen from Fig. 4 that when the external excitation frequency approaches steady values of the first, second, and third natural frequency, the main resonance of the jet system is strong, and the amplitudes of the fluid unit 1, the spray core and the fluid unit 2 reach the maximum respectively, which is closely related to the modal characteristics of the jet system. It can be seen from Fig. 5 that when the main resonance occurs, the external excitation frequency is the dominant frequency. From (25) and (26), it can be known that the main resonance response also includes the combined frequency between the natural frequency of each order and the equivalent stiffness fluctuation frequency of the fluid unit. Since the external excitation frequency is smaller than the combined frequency, the combined frequency has less effect on the main resonance of the jet system, but it still has a regulating effect. When the external excitation frequency is equal to the first natural frequency, the amplitude of the main resonance is the largest, which is 0.2592 mm.

B. ANALYSIS OF THE COMBINED RESONANCE RESPONSE OF JET SYSTEM

When the external excitation frequency is close to the sum of the stable values of the natural angular frequency of each order and the equivalent stiffness fluctuation angular frequency of the fluid unit, the time domain response and the frequency domain response of the jet system are shown in Fig. 6 and Fig. 7, respectively.

It can be seen from Fig. 6 that when the external excitation frequency is close to the combined frequency, the combined resonance occurs in the jet system and the amplitude is relatively large, but the amplitude is smaller than that in the main resonance. It can be seen from Fig. 7 that when the combined resonance occurs in the jet system, the dominant frequency is the combined frequency, and the natural frequency of each order has effects of regulation. Meanwhile, it can be found that when the external excitation frequency is the sum of the first and second natural frequency and the fluid stiffness fluctuation frequency, respectively, the displacements of the fluid unit 1 and the spray core reach the maximum, and when the external excitation frequency is the sum of the third natural
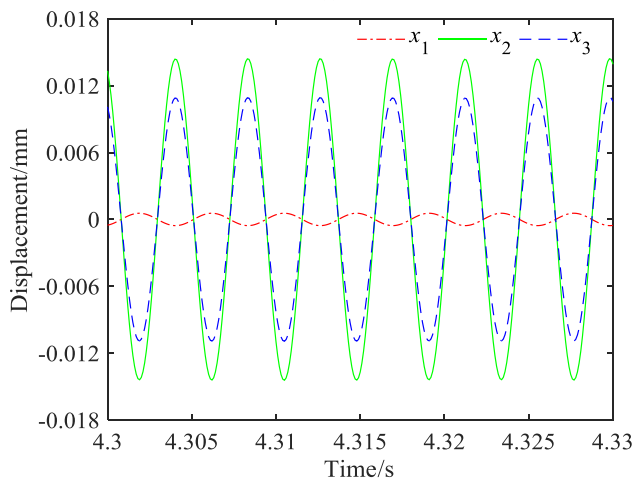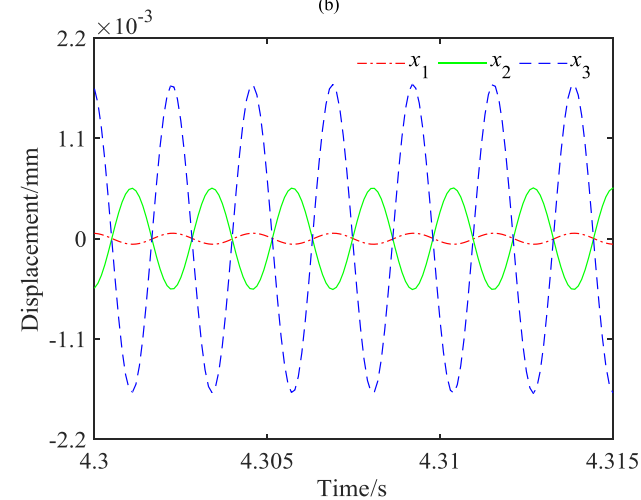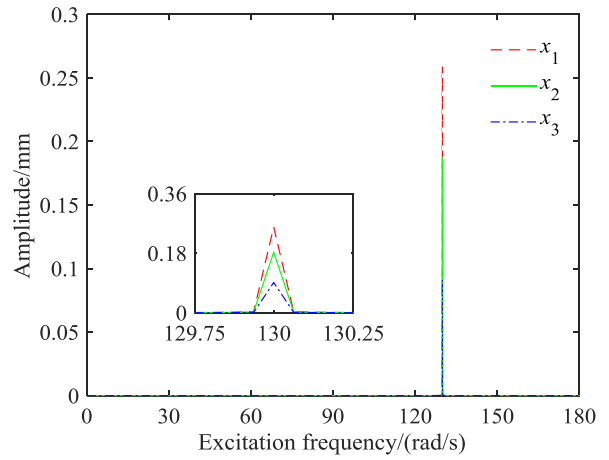
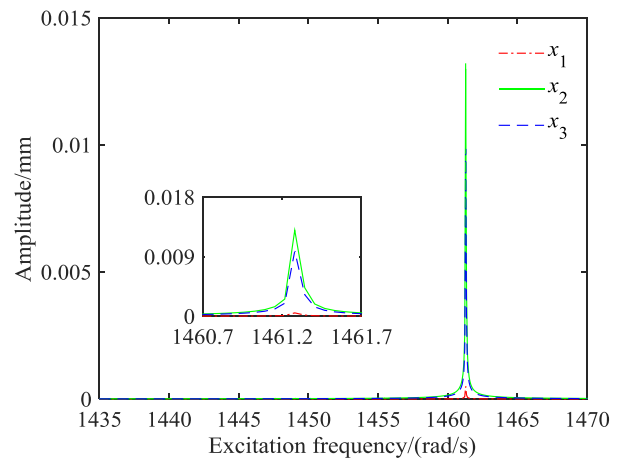**FIGURE 4.** Time domain response of the main resonance of jet system when $\omega_o \approx \omega_{ni}$. **(a)** $\omega_o \approx \omega_{n1}$. **(b)** $\omega_o \approx \omega_{n2}$. **(c)** $\omega_o \approx \omega_{n3}$.
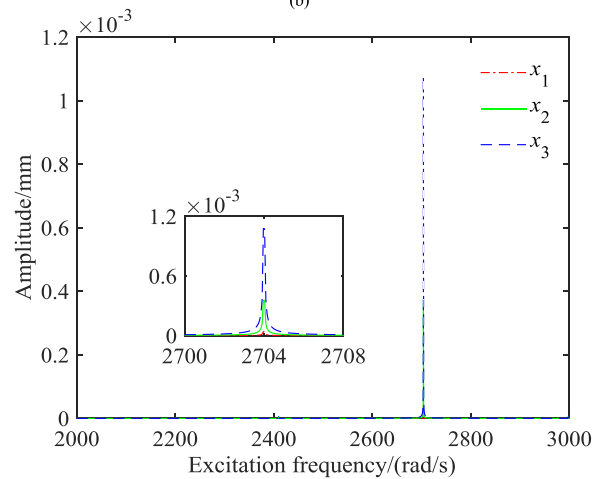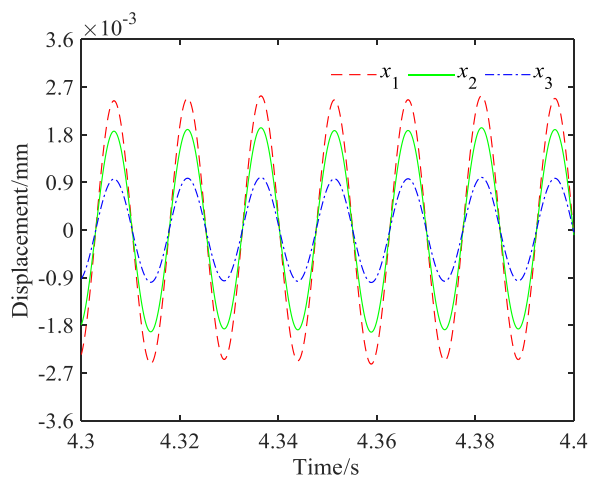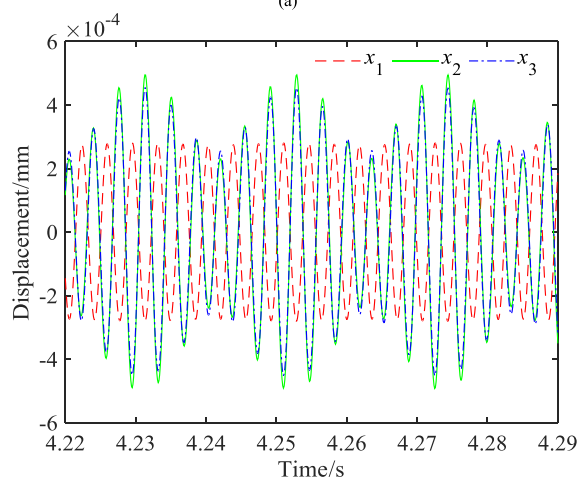

FIGURE 5. Frequency domain response of the main resonance of jet system when $\omega_o \approx \omega_{ni}$. **(a)** $\omega_o \approx \omega_{n1}$. **(b)** $\omega_o \approx \omega_{n2}$. **(c)** $\omega_o \approx \omega_{n3}$.

frequency and fluid stiffness fluctuation, the displacement of the fluid unit 1 is the largest. When the external excitation frequency is the sum of the first natural frequency and the

fluid stiffness fluctuation frequency, the amplitude of the combined resonance is the largest, which is 0.002532 mm.
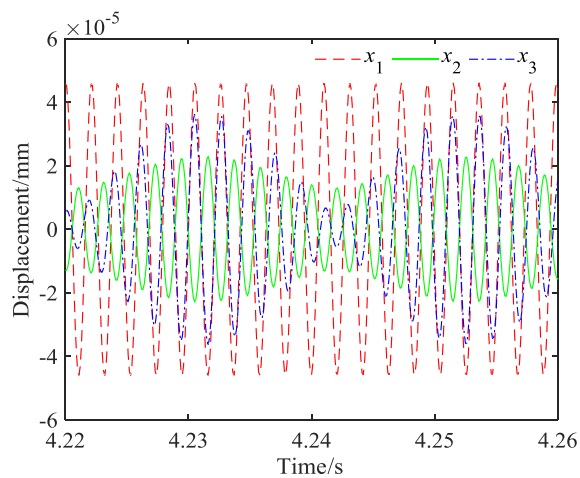
V. EXPERIMENTAL VERIFICATION
In order to verify the accuracy of the dynamic model of the adaptive gun head jet system of the fire-fighting monitor,
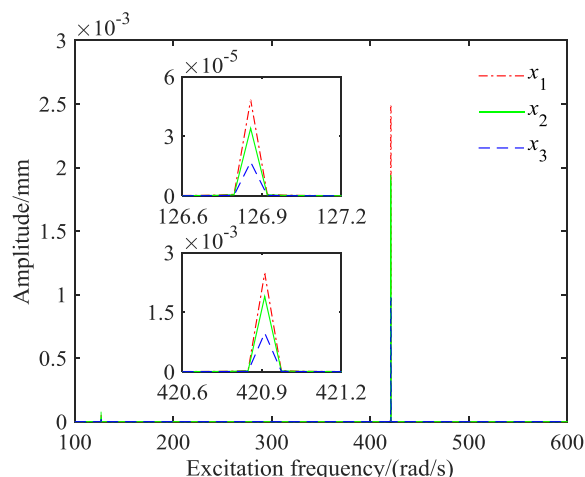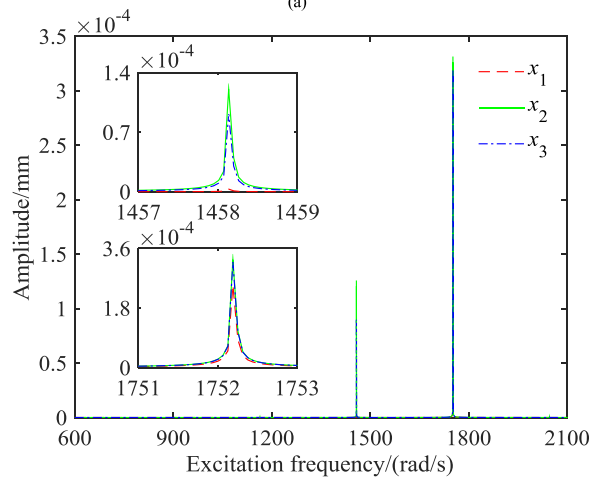
FIGURE 6. Time domain response of the combined resonance of jet system when $\omega_o \approx \omega_i + \omega_f$. **(a)** $\omega_o \approx \omega_{n1} + \omega_f$. **(b)** $\omega_o \approx \omega_{n2} + \omega_f$. **(c)** $\omega_o \approx \omega_{n3} + \omega_f$.

FIGURE 7. Frequency domain response of the combined resonance of jet system when $\omega_o \approx \omega_{ni} + \omega_f$. **(a)** $\omega_o \approx \omega_{n1} + \omega_f$. **(b)** $\omega_o \approx \omega_{n2} + \omega_f$. **(c)** $\omega_o \approx \omega_{n3} + \omega_f$.
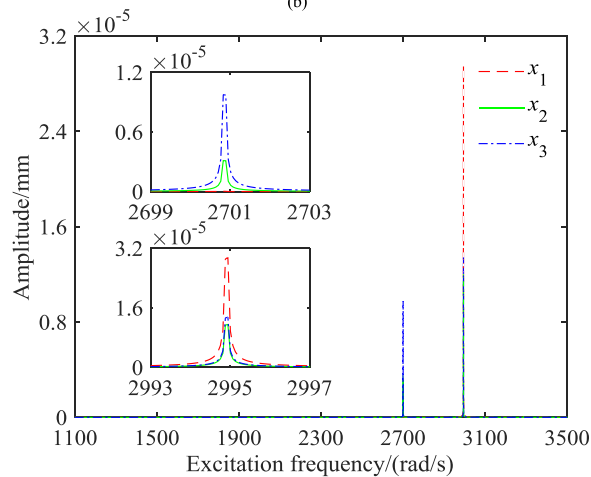
a modal test is required, which can be divided into two parts, namely the fluid pressure pulsation modal analysis and the jet system modal analysis.

A. MODAL ANALYSIS OF THE FLUID PRESSURE PULSATION

Due to the pressure pulsation of the fluid caused by the centrifugal pump, the bulk modulus of the fluid unit in the jet system changes dynamically, which exacerbates the
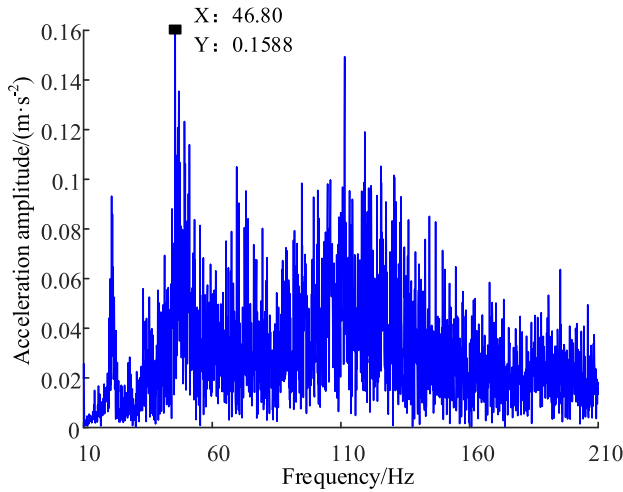
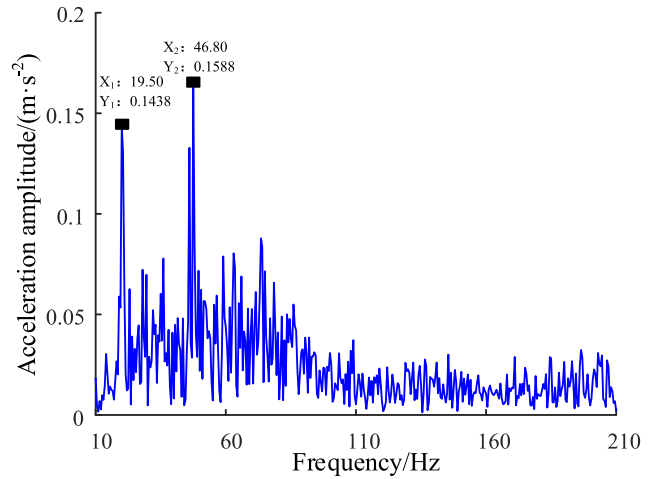**FIGURE 8.** Curve of fluid pressure pulsation amplitude-frequency characteristic.
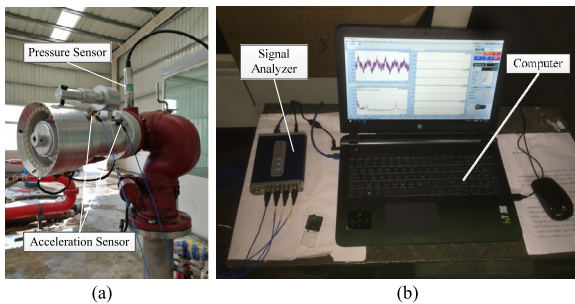

FIGURE 9. Platform for dynamic experiment of the adaptive gun head jet system of the fire-fighting monitor. (a) prototype of gun head. (b) experimental equipment.

complexity of the dynamics of the jet system. In order to determine the pressure pulsation frequency of the input fluid during the experiment, the amplitude-frequency characteristics of the fluid pressure signal are analyzed, and the cause of frequency components is not discussed here. The amplitude-frequency characteristics of the fluid pressure pulsation are shown in Fig. 8.

It can be seen from Fig. 8 that the amplitude-frequency characteristic curve of the fluid pressure pulsation has a peak at 46.8 Hz, and this frequency corresponds to the shaft frequency (2800 RPM) of the centrifugal pump, so the pressure pulsation frequency of the fluid in the jet system is 46.8 Hz. In addition, the turbulence in the jet system introduces white noise components, leading amplitude-frequency characteristic curve to be very complicated as a whole.

B. MODAL ANALYSIS OF JET SYSTEM

A platform for the dynamic experiment of the jet system was built and the modal test was carried out by the hammering method. The experiment platform is shown in Fig. 9.

The fast Fourier transform is used to analyze the acceleration signal output from the jet system in the frequency domain. The amplitude-frequency characteristics of the acceleration signal of the jet system under the superposition

FIGURE 10. Curve of amplitude-frequency characteristic of the adaptive gun head jet system of the fire-fighting monitor.

TABLE 3. Comparison between experimental data and theoretical value.

Natural frequency	Experimental data/Hz	Theoretical value/Hz	Error/%
The first natural frequency	19.5	19.67	0.87

of the fluid pulsation excitation and the hammer step excitation are shown in Fig. 10.

It can be seen from Fig. 10 that the jet system has peaks at 19.5 Hz and 46.8 Hz. Since the excitation of the jet system at this time is the superposition of the hammer step excitation and the fluid pulsation excitation, and the fluid pulsation frequency is 46.8 Hz, the experimental value of the first natural frequency is 19.5Hz. Since the natural frequencies of the other orders of the jet system are relatively high, and are far from the external excitation frequency, and the high-frequency part is chaotic under the influence of turbulence, the natural frequencies of other orders are not analyzed for the time being. The experimental data and theoretical value of the first natural frequency of the jet system are shown in Table 3.

It can be seen from Table 3 that the theoretical value of the first natural frequency of the jet system is very close to the experimental one, and the error is small, which illustrates the validity and accuracy of the theoretical analysis of the dynamics of the jet system.

VI. CONCLUSIONS

Due to the pressure pulsation of the fluid, the adaptive gun head jet system of the fire-fighting monitor is a typical parametric vibration system. When the pulsation excitation frequency is close to the natural frequency of the jet system or the combined frequency between the natural frequency and the equivalent stiffness fluctuation frequency of the fluid unit, the main resonance or combined resonance of the jet system will occur. Resonance will seriously deteriorate the dynamic behaviors of the jet system, and the jet system has the following vibration characteristics:

1. The dominant frequency of the main resonance response is the external excitation frequency of the jet system, and the combined frequency has a small effect of regulation on the main resonance of the jet system. When the external excitation frequency is equal to the first natural frequency, the amplitude of the main resonance is the largest, which is 0.2592 mm.

2. When the external excitation frequency is close to the combined frequency, the amplitude is smaller than that in the main resonance. The dominant frequency is the combined frequency, and the natural frequency of each order has effects of regulation. When the external excitation frequency is the sum of the first and second natural frequency and the fluid stiffness fluctuation frequency, respectively, the displacements of the fluid unit 1 and the spray core reach the maximum. When the external excitation frequency is the sum of the third natural frequency and fluid stiffness fluctuation, the displacement of the fluid unit 1 is the largest. When the external excitation frequency is the sum of the first natural frequency and the fluid stiffness fluctuation frequency, the amplitude of the combined resonance is the largest, which is 0.002532 mm.

3. A platform for the dynamic experiment of the adaptive gun head jet system of the fire-fighting monitor was built and the modal test was carried out. The experimental value of the first natural frequency of the jet system is very close to the theoretical one, and the error is small, which illustrates the validity and accuracy of the theoretical analysis of the dynamics of the jet system.

REFERENCES

[1] X. Yuan, X. Zhu, C. Wang, L. Zhang, and Y. Zhu, "Natural frequency sensitivity analysis of fire-fighting jet system with adaptive gun head," *Processes*, vol. 7, no. 11, p. 808, 2019.

[2] X. Yuan, X. Zhu, C. Wang, and L. Zhang, "Research on theoretical model of dynamic bulk modulus of gas-containing hydraulic oil," *IEEE Access*, vol. 7, pp. 178413–178422, 2019.

[3] S. Tang, S. Yuan, and Y. Zhu, "Deep learning-based intelligent fault diagnosis methods toward rotating machinery," *IEEE Access*, vol. 8, pp. 9335–9346, 2020.

[4] Y. Zhu, S. Tang, L. Quan, W. Jiang, and L. Zhou, "Extraction method for signal effective component based on extreme-point symmetric mode decomposition and Kullback–Leibler divergence," *J. Brazilian Soc. Mech. Sci. Eng.*, vol. 41, no. 2, pp. 1–11, Feb. 2019.

[5] W. Li, E. Li, L. Ji, L. Zhou, W. Shi, and Y. Zhu, "Mechanism and propagation characteristics of rotating stall in a mixed-flow pump," *Renew. Energy*, vol. 153, pp. 74–92, Jun. 2020.

[6] Q. Gao, J. Ye, B. Wang, and J. Zhao, "Investigation of unsteady pressure pulsation and internal flow in a centrifugal pump under low flow rate," *Int. J. Fluid Machinery Syst.*, vol. 12, no. 3, pp. 189–199, Sep. 2019.

[7] N. Zhang, B. Gao, X. Wang, X. Liu, and D. Ni, "Effects of cutting the blade on the performance and pressure pulsation of a centrifugal pump," *Energy Sci. Eng.*, Jan. 2020, doi: 10.1002/ese3.608.

[8] J. Zhang, D. Appiah, F. Zhang, S. Yuan, Y. Gu, and S. N. Asomani, "Experimental and numerical investigations on pressure pulsation in a pump mode operation of a pump as turbine," *Energy Sci. Eng.*, vol. 7, no. 4, pp. 1264–1279, Aug. 2019.

[9] X. Yuan, X. Zhu, C. Wang, L. Zhang, and Y. Zhu, "Research on the dynamic behaviors of the jet system of adaptive fire-fighting monitors," *Processes*, vol. 7, no. 12, p. 952, 2019.

[10] L. Xu and Y. Gao, "Bifurcation and chaotic vibration in electromechanical integrated toroidal drive," *J. Vibrat. Control*, vol. 21, no. 8, pp. 1556–1565, Jun. 2015.

[11] Y. Zhu, S. Tang, C. Wang, W. Jiang, X. Yuan, and Y. Lei, "Bifurcation characteristic research on the load vertical vibration of a hydraulic automatic gauge control system," *Processes*, vol. 7, no. 10, p. 718, 2019.

[12] Y. Zhu, P. Qian, S. Tang, W. Jiang, W. Li, and J. Zhao, "Amplitude-frequency characteristics analysis for vertical vibration of hydraulic AGC system under nonlinear action," *AIP Adv.*, vol. 9, no. 3, Mar. 2019, Art. no. 035019.

[13] Y. Qiang, Y. Qian, and X. Guo, "Periodic solutions of delay nonlinear system by multi-frequency homotopy analysis method," *J. Low Freq. Noise, Vibrat. Act. Control*, vol. 38, nos. 3–4, pp. 1439–1454, Dec. 2019.

[14] C. Liu, X. Deng, J. Liu, and Z. Zheng, "Impact-induced nonlinear damped vibration of fabric membrane structure: Theory, analysis, experiment and parametric study," *Compos. B, Eng.*, vol. 159, pp. 389–404, Feb. 2019.

[15] M. M. Keleshteri and J. Jelovica, "Nonlinear vibration behavior of functionally graded porous cylindrical panels," *Compos. Struct.*, vol. 239, May 2020, Art. no. 112028, doi: 10.1016/j.compstruct.2020.112028.

[16] G.-X. Wang, H. Ding, and L.-Q. Chen, "Dynamic effect of internal resonance caused by gravity on the nonlinear vibration of vertical cantilever beams," *J. Sound Vibrat.*, vol. 474, May 2020, Art. no. 115265.

[17] M. Sadri, D. Younesian, and E. Esmailzadeh, "Nonlinear harmonic vibration and stability analysis of a cantilever beam carrying an intermediate lumped mass," *Nonlinear Dyn.*, vol. 84, no. 3, pp. 1667–1682, May 2016.

[18] J. Armand, L. Pesaresi, L. Salles, C. Wong, and C. W. Schwingshackl, "A modelling approach for the nonlinear dynamics of assembled structures undergoing fretting wear," *Proc. Roy. Soc. A, Math., Phys. Eng. Sci.*, vol. 475, no. 2223, Mar. 2019, Art. no. 20180731.

[19] X. H. Hao, H. Q. Zhu, and D. Pan, "Nonlinear resonance responses of electromechanical integrated magnetic gear system," *Shock Vib.*, vol. 2018, Mar. 2018, Art. no. 9821870.

[20] X. Hao and X. Zhu, "Nonlinear forced vibration of electromechanical integrated magnetic gear system," in *Proc. IEEE Int. Conf. Mechatronics Autom. (ICMA)*, Aug. 2015, pp. 612–617.

[21] Z. Odibat, "On the optimal selection of the linear operator and the initial approximation in the application of the homotopy analysis method to nonlinear fractional differential equations," *Appl. Numer. Math.*, vol. 137, pp. 203–212, Mar. 2019.

[22] G. Larriccio, A. Zippo, F. Pellicano, and M. Barbieri, "Resonances and nonlinear vibrations of circular cylindrical shells, effects of thermal gradients," *Proc. Inst. Mech. Eng., C, J. Mech. Eng. Sci.*, Mar. 2020, doi: 10.1177/0954406220907616.

[23] Zhu, Tang, Wang, Jiang, Zhao, and Li, "Absolute stability condition derivation for position closed-loop system in hydraulic automatic gauge control," *Processes*, vol. 7, no. 10, p. 766, 2019.

[24] L. Lyu, Z. Chen, and B. Yao, "Energy saving motion control of independent metering valves and pump combined hydraulic system," *IEEE/ASME Trans. Mechatronics*, vol. 24, no. 5, pp. 1909–1920, Oct. 2019.

[25] L. Lyu, Z. Chen, and B. Yao, "Advanced valves and pump coordinated hydraulic control design to simultaneously achieve high accuracy and high efficiency," *IEEE Trans. Control Syst. Technol.*, Feb. 25, 2020, doi: 10.1109/TCST.2020.2974180.

[26] J. Yao and W. Deng, "Active disturbance rejection adaptive control of hydraulic servo systems," *IEEE Trans. Ind. Electron.*, vol. 64, no. 10, pp. 8023–8032, Oct. 2017.

[27] Z. Yao, J. Yao, and W. Sun, "Adaptive RISE control of hydraulic systems with multilayer neural-networks," *IEEE Trans. Ind. Electron.*, vol. 66, no. 11, pp. 8638–8647, Nov. 2019.

[28] L. Lyu, Z. Chen, and B. Yao, "Development of pump and valves combined hydraulic system for both high tracking precision and high energy efficiency," *IEEE Trans. Ind. Electron.*, vol. 66, no. 9, pp. 7189–7198, Sep. 2019.

XIAOMING YUAN received the B.S. and Ph.D. degrees from the School of Mechanical Engineering, Yanshan University, Qinhuangdao, China, in 2008 and 2014, respectively. He held a Postdoctoral position with XCMG Construction Machinery, from 2015 to 2018. Since 2015, he has been a Lecturer with the School of Mechanical Engineering, Yanshan University. His research interests include fluid-structure interaction dynamics of fire-fighting monitor, fluid transmission and control, and new magnetic gear transmission and control. He is a Senior Member of the Chinese Mechanical Engineering Society (CEMS).

XUAN ZHU received the B.S. degree from the School of Mechanical Engineering, Yanshan University, Qinhuangdao, China, in 2018, where he is currently pursuing the master's degree. His research interests include fluid transmission and control and fluid system simulation.
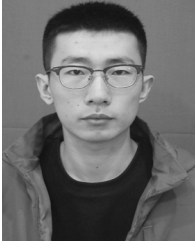
CHU WANG received the B.S. degree from the College of Mechatronic Engineering, North University of China, Taiyuan, China, in 2017. He is currently pursuing the master's degree with the School of Mechanical Engineering, Yanshan University, Qinhuangdao, China. His research interests include fluid transmission and control and fluid system simulation.

LIJIE ZHANG received the B.S., M.S., and Ph.D. degrees from the School of Mechanical Engineering, Yanshan University, Qinhuangdao, China. He has been a Professor with the School of Mechanical Engineering, Yanshan University, since 2008, and became a Doctoral Tutor, in 2008. He was a Senior Visiting Scholar with the Iowa State University of Science and Technology, in 2009. His research interests include the reliability and fault diagnosis of hydraulic components, multiphysics coupling analysis, and mechanics and robotics. He is a Senior Member of the Chinese Mechanical Engineering Society (CEMS) and a Review Expert of the National Natural Science Foundation of China (NSFC).

• • •